Appl Phys A (2009) 94: 221–230
DOI 10.1007/s00339-008-4859-6

Applied Physics A
Materials Science & Processing

RAPID COMMUNICATION

Nanostructuring of thin gold films by femtosecond lasers

A.I. Kuznetsov · J. Koch · B.N. Chichkov

Received: 22 July 2008 / Accepted: 1 August 2008 / Published online: 15 August 2008
© Springer-Verlag 2008

Abstract Novel experimental data on microstructuring of thin (60 nm) gold films by femtosecond laser pulses are presented and discussed. Material modifications are induced by different laser field distributions on the sample surface. Images of specially fabricated masks are transferred onto the gold surface with a 50× and 100× demagnifications. It is shown that, in the irradiated region of the gold film, the heated material tends to concentrate in the center. For example, a square-like field distribution on the target surface produces a cross with a jet in the middle. It is shown that this technique allows producing of a variety of microstructures with controllable nanorelief. Possible mechanisms leading to the observed material modifications as well as the resolution limits of this technique are discussed.

PACS 42.62._b · 42.65.Re · 68.15._e

1 Introduction

Femtosecond (fs) lasers have proved to be a powerful tool for surface and volume structuring of different materials. Size of the fs laser-created structures can be well below the irradiation wavelength due to ultra-fast material excitation, excellent control of the deposited energy, and different possibilities for nonlinear material modifications [1–3].

Laser processing of thin metal films attracts considerable attention because of a wide variety of structures, which can be obtained due to complicated laser-induced melt and solidification dynamics [4–17]. Laser ablation of thin metal films is also considered as a promising approach to microstructuring [18–20]. Thin gold films can be structured below the ablation threshold by irradiation with nanosecond [4–6] and femtosecond [7–10] laser pulses. It was shown that, while under nanosecond laser irradiation material melt dynamics is a dominant process, femtosecond irradiation induces more complicated dynamics including film deformations. Nanosecond laser-induced melt of thin gold films demonstrates different behavior depending on film thickness and material purity. For example, in thinner gold films (20–50 nm) redistribution of the laser-melted material from "hot" (irradiated) to "cold" (not irradiated) domains was demonstrated [4]. This was applied for microstructuring of gold films using interfering laser beams. On the other hand, in thicker gold films (60–120 nm) the "pileup" of the material in the center of the irradiated region was observed [5, 6]. This was explained by the presence of impurities inside the film, while pure gold should move in the opposite direction due to shear forces caused by the laser-induced gradient in surface tension [11]. However, the nature of such impurities in the gold films is not clear. Films thinner than 10 nm melted by laser irradiation tend to break up into separate melted drops (dewetting) forming self-organized nanostructures [4, 12–14].

Femtosecond laser-induced processes inside thin gold films are rather complicated. They include not only material melt dynamics but also film deformation as a whole. Typical structure that occurs on the gold film surface under irradiation by a single femtosecond laser pulse with the Gaussian intensity profile is shown in Fig. 1(a) and 1(b). It consists of a hollow microbump with a nanojet on it [7–10]. As it was shown in previous publications, the bump appears first at relatively low laser energies (Fig. 1(a)) and starts

A.I. Kuznetsov (✉) · J. Koch · B.N. Chichkov
Laser Zentrum Hannover e.V., Hollerithalle 8, 30419 Hannover, Germany
e-mail: a.kuznetsov@lzh.de
Fax: +49-511-2788100

to grow with increasing laser intensity. At certain threshold laser pulse energy, the nanojet appears on the top of the bump (Fig. 1(b)) and grows further with the laser intensity [7, 8]. Different models have been proposed to explain the formation of these structures on the gold film surface: thermoplastic deformation of the film [21], Marangoni convection flow of the melted material [7], evaporation of gold under the film [10], and photomechanical spallation [22].

In this paper, modification of 60 nm gold films under irradiation by femtosecond laser pulses having different micro-intensity distributions is studied. For this purpose, images of specially fabricated masks are transferred onto the gold surface with a 50× demagnification. It is shown that a variety of microstructures with controlled nanorelief can be created on the gold surface using this technique. Possible mechanisms which could be responsible for the observed material modifications as well as the resolution limits of this technique are discussed.

2 Experimental details

In our experiments, we use a commercial 1 kHz femtosecond laser system (Femtolasers Produktions GmbH Femtopower Compact Pro) delivering 0.9 mJ, 30 fs laser pulses at average wavelength of 800 nm. Gold films with a 60 nm thickness coated onto quartz glass substrates were fabricated by Layertec GmbH using magnetron sputtering.

The image transfer scheme with a 50× demagnification has been realized using 50× Nikon long-distance microscope objective with a numerical aperture (NA) of 0.45 and working distance of 13.8 mm and additional lens with a focal distance $f = 200$ mm. In some experiments, a 100× Zeiss microscope objective (Epilan-Neofluar, NA 0.9) and a lens with the focal distance $f = 164.5$ mm were also used to realize image transfer scheme with 100× demagnification. Focus distances of the used lenses are the same as of the tube lenses used in the microscopes, that allows corresponding image transfer. To create different micro-field distributions on the sample surface, images of different masks have been transferred. These masks have been fabricated by femtosecond pulse laser ablation of a 100 nm chromium film deposited on a glass substrate. Very clean ablation of Cr films has been realized by a train of 30 fs laser pulses focused with a 60 mm achromatic lens with the following processing parameters: laser pulse energy $E_p = 0.8$ μJ, repetition rate of 1 kHz, and the sample translation velocity of 100 μm/s.

Laser-induced gold structures have been analyzed by Scanning Electron Microscopy (SEM) and Atomic Force Microscopy (AFM).

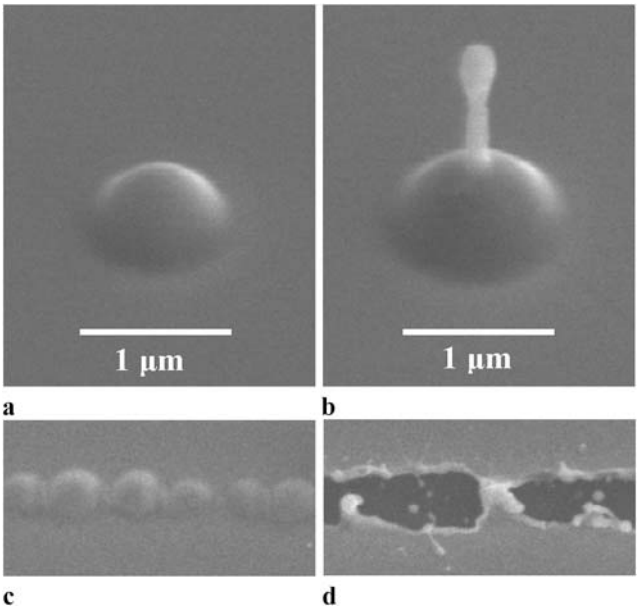

Fig. 1 (**a**) and (**b**) Microbump and nanojet structures fabricated by single tightly focused femtosecond laser pulses with the pulse energies of 30 nJ and 50 nJ, respectively. (**c**) Microbumps, separated by a distance of 0.7 μm, fabricated by a sequence of 30 nJ laser pulses. (**d**) Structure produced by a sequence of laser pulses with the same energy as in (**c**) but separated by 0.5 μm

3 Results and discussion

In this experiment, laser pulses have been focused on the sample surface with a 50× Nikon long-distance microscope objective with NA of 0.45. The nanojet structures created on the gold film surface by a single laser pulse with the Gaussian intensity distribution have characteristic sizes, much lower than the laser wavelength (800 nm) (Fig. 1(b)). Controlled changing of this nanorelief by varying laser irradiation parameters seems to be interesting for different applications. However, structuring of the gold film surface by multiple laser pulses is limited to the fabrication of well separated microbumps/nanojet structures, while intersection of these structures leads to the rupture of the film (see examples in Fig. 1(c) and (d)). One can expect that nanorelief of the created structures can be controlled by the laser pulse intensity distribution on the target surface. On the other hand, studying of the modification morphology under different laser field distributions can provide new insights into the involved laser–matter interactions.

3.1 Laser-induced material modifications

Figure 2 shows a line-like gold film modification, which was obtained by irradiation of the sample using a single femtosecond laser pulse with an intensity distribution strongly elongated perpendicular to the beam axes. To obtain this field distribution on the sample surface, the beam was directed onto a slit diaphragm with a slit width of 150 μm and

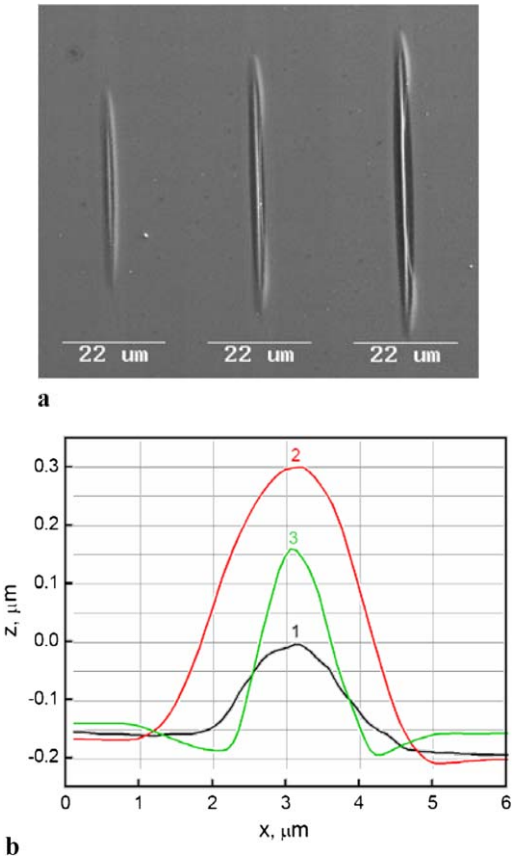

Fig. 2 Line-like material modifications obtained after irradiation of a 60 nm gold film by single femtosecond laser pulses with an elongated intensity distribution. The laser beam with the diameter of 8 mm was directed onto the 150 μm slit and then focused onto the sample surface with a 20 mm achromatic lens: (**a**) SEM images for the pulse energies measured before the slit of 110 μJ, 120 μJ, and 130 μJ, respectively; (**b**) profiles of the line structures measured by AFM. The laser fluences corresponding to these profiles are: $F_1 < F_2 < F_3$

then focused by a 20 mm lens. One can see that a straight line of the piled up material is obtained on the sample surface. However, this material modification is different from that obtained with a tightly focused Gaussian beam. At sufficiently high intensities the structure profile as demonstrated in Fig. 2(b) (curve 3) shows decrease of the gold film thickness at the line edge. One can state that redistribution of material from the edge to the central region of the irradiated line occurs. However, this process cannot be explained only by the flow of melted material, because simple volumetric estimations show that the bump in the center of the line is hollow inside. This can be attributed to the complex process of a simultaneous film deformation and partial melting, which will be discussed further in this paper.

In order to clarify the mechanism of the laser-induced structure formation, different model laser intensity distributions have been created on the sample surface. For this purpose, an image transfer scheme with a 50× demagnification has been applied. Masks of different shapes with the structural sizes from several tens up to several hundreds of micrometers were fabricated by laser ablation of chromium films deposited on glass substrates. Image transfer of these masks with a 50× demagnification allows creation of different micrometer size laser intensity distributions on the sample surface.

Figure 3 demonstrates SEM images of the structures fabricated on the gold film surface by a single femtosecond laser pulse with a square-shaped intensity distribution. One can see that at smaller laser fluences a pyramidal shape bump appears on the sample surface (Fig. 3(a)). At higher laser fluences the material starts to concentrate in the central region forming thereby a cross with a jet in the middle (Fig. 3(b)). An important peculiarity of the jet is a droplet on the top. This droplet becomes bigger at higher laser fluences as well as the whole jet, while the film becomes thinner at the edges of the irradiated area (Fig. 3(c)). Observation of the droplet on the top of the jet indicates the presence of the melted phase during the modification process. It should be noted that the transition between the microbump and the cross structures is threshold-like and occurs within only 2% variation of the laser fluence.

Important feature of the both types of structures shown in Fig. 2 and Fig. 3 is redistribution of the material from the edges to the center of the irradiated area. This process was not clearly observed in earlier experiments [7, 8] with tightly focused Gaussian laser pulses. However, this difference in the material behavior can be attributed not only to the intensity distribution but rather to the size of the fabricated structures. Indeed, the characteristic size of the irradiated region in Fig. 2 and Fig. 3 is several micrometers, while in Fig. 1 and in [7] and [8] it is smaller than one micrometer. In order to verify this hypothesis, the sample was irradiated by a Gaussian beam with a larger focus diameter (Fig. 4). For this purpose the laser beam was focused onto the sample surface by a 20 mm achromatic lens. One can see in Fig. 4(d) that in this case the redistribution of the material from the edges to the center of the irradiated area also occurs at sufficiently high laser fluences. Moreover, the form of the jet structure fabricated at these energies (Fig. 4(d)) is very similar to that obtained with a square-shaped laser intensity distribution (Fig. 3(c)). The jet structures in Figs. 3(c) and 4(d) have three similar characteristic features: a droplet on the top, a column in the middle, and a disk at the bottom. All these three features are very reproducible and appear apparently due to the melted material dynamics and solidification.

As it was mentioned above, the redistribution of the material from the edges to the center of the irradiated area is most likely due to the melted material dynamics. A strong indication of presence of the melted phase is the droplet formation on the top of the jet structure. Dynamics of gold films melted by *nanosecond* laser irradiation was earlier described in several publications [4–6, 23–26]. It was shown that the melted

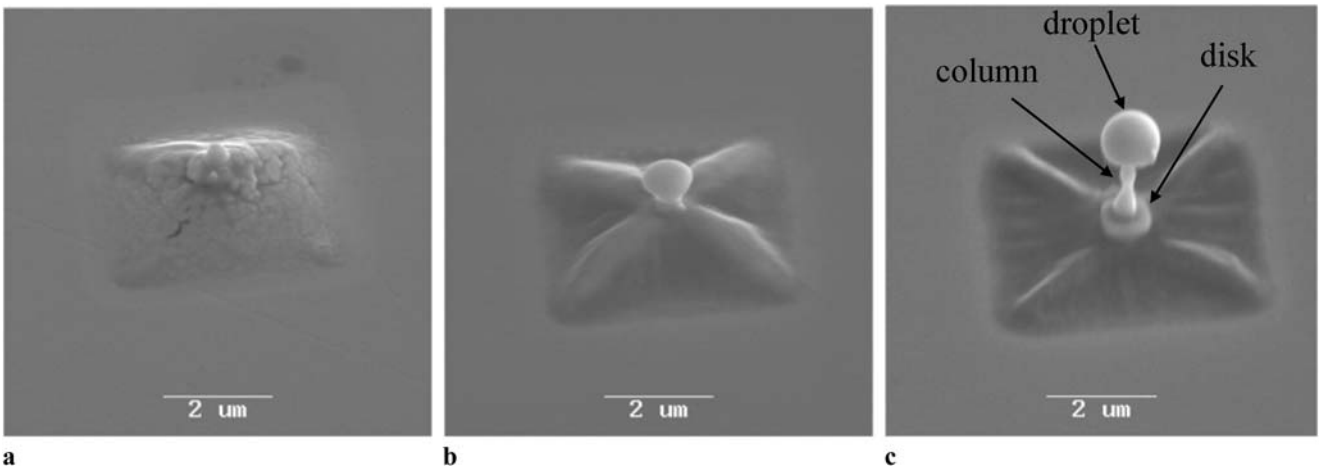

Fig. 3 Structures obtained by irradiation of a 60 nm gold film with single femtosecond laser pulses having square-shaped intensity distribution. The laser fluences on the sample surface are 0.19 J/cm^2 (**a**), 0.195 J/cm^2 (**b**), and 0.2 J/cm^2 (**c**)

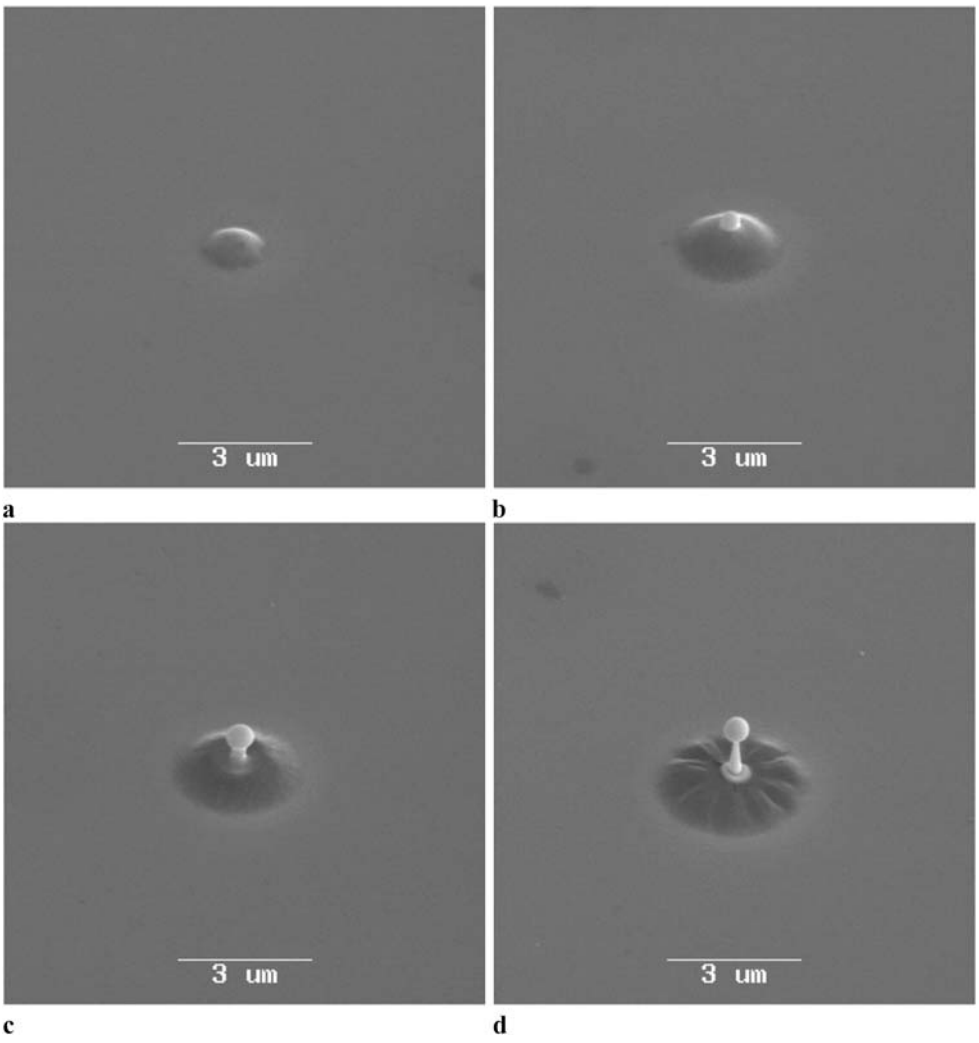

Fig. 4 Structures obtained by irradiation of a 60 nm gold film with single femtosecond laser pulses. The laser beam with the diameter of 8 mm has been focused on the sample surface with a 20 mm achromatic lens. The laser pulse energies were 40 nJ (**a**), 46 nJ (**b**), 58 nJ (**c**), and 78 nJ (**d**)

material dynamics depends on the film thickness and gold purity. The authors of [4] show that when a thin gold film (20–50 nm) is melted by *nanosecond* laser irradiation, the material tends to redistribute from the hot/irradiated regions to the cold/unirradiated regions. This melted material behavior is due to the gradients in the surface tension caused by

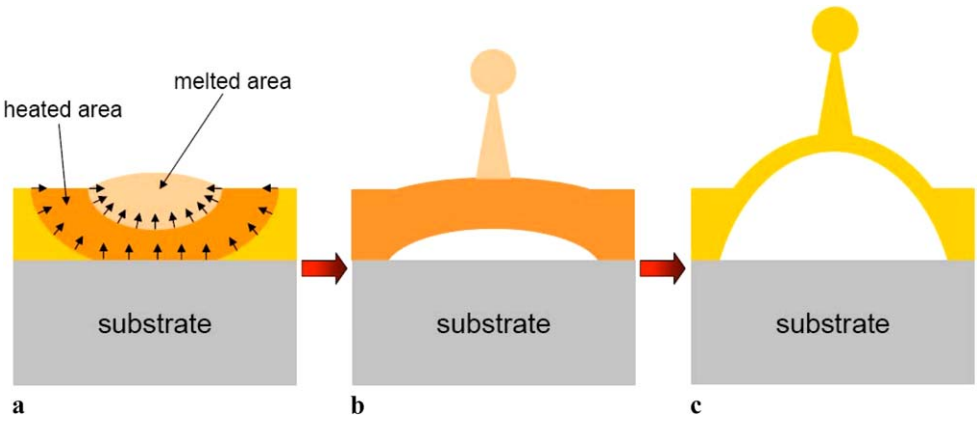

Fig. 5 Schematic illustration of the mechanisms responsible for the structure formation

the inhomogeneous laser-induced material temperature distribution: $\partial\sigma/\partial x = (\partial\sigma/\partial T) \times (\partial T/\partial x)$, where σ is the surface tension, T is the temperature, and x is a coordinate. For pure liquid gold as well as for other pure liquid metals, the thermal coefficient $\partial\sigma/\partial T$ is negative and provides forces pushing the material from the hot to the cold region. Similar dynamics of melted material under *nanosecond* laser irradiation was also observed for several other metals [11, 27, 28]. On the other hand, the authors of [5] and [6] have observed that when a 60 nm gold film is melted by *nanosecond* laser irradiation, the melted material tends to concentrate in the center of the irradiated region after a single laser pulse. This different behavior is explained by the presence of surface impurities, which can change the sing of the surface tension gradient. However, the nature of such impurities in a gold film is still unclear. In [5] and [6], it was also shown that the laser pulse can clean the gold film surface from impurities, and if the second laser pulse irradiates the same sample point after a several microseconds delay it can induce reversal flow of the melted material from the center to the edges of the irradiated region. This reversal flow is not observed when the delay between the pulses is on the order of seconds or longer.

On the other hand, in [23] and [24], it was suggested that the gold melted by the laser irradiation can redistribute to the center of the irradiated region due to the thermal expansion of the heated solid part of the material. This process provides forces acting on the melted gold at the solid–liquid interface. These forces are directed perpendicularly to the interface and push the liquid phase from the solid (see Fig. 5(a)). In case of material melted by a laser beam with the Gaussian intensity distribution, these forces push the melted material into the center of the irradiated region. Another important point is that the liquid gold has lower density (compared to solid) and thus the phase transition leads to the material expansion and provides additional forces acting in the same direction. This model has been applied to explain experimental data on droplet formation under multi-pulse nanosecond laser irradiation of a gold target during laser sputtering [25, 26]. Though under the sputtering conditions the droplets are formed by multiple laser pulses, in [23] and [24], it was suggested that the droplets can also be formed by a single laser pulse with higher laser intensity. Apparently, this mechanism can also work in case of *femtosecond* laser irradiation of thin gold films. One can expect that in case of *femtosecond* laser processing these forces will be even more significant due to faster material heating, which proceeds at picoseconds, and thus faster thermal expansion and phase transition.

Femtosecond laser irradiation of 60 nm gold films induces melted material flow from the edges to the center of the irradiated region. This material behavior can be explained by two different mechanisms earlier proposed for *nanosecond* laser processing: the thermal expansion-induced stress and the impurity-dependent surface tension gradients. To distinguish between these two possible mechanisms additional experiments were carried out. The same position at the gold surface was irradiated by two subsequent femtosecond laser pulses. Two different time delays between the pulses have been introduced: 1 ms and 3 s. According to [5, 6], in case of a small delay between two laser pulses, the first pulse cleans the surface eliminating impurities. Therefore, if the melt dynamics is governed by the impurity-dependent surface tension gradients, after the second pulse the material should move to the edges of the irradiated region. The obtained experimental results are shown in Fig. 6. One can see that no material flow to the edges of the irradiated region is observed. Moreover, material tends to concentrate further in the center forming a well defined droplet, while the film is completely melted and broken after the second laser pulse. It is also seen that the delay between the laser pulses does not significantly affect the melted material dynamics. According to these experimental results, one can conclude that the stress induced by the thermal expansion of the solid and liquid materials seems to be the dominant mechanism responsible for the melted material flow to the center of the irradiated region under femtosecond laser irradiation. On the other hand the complicated shape of the

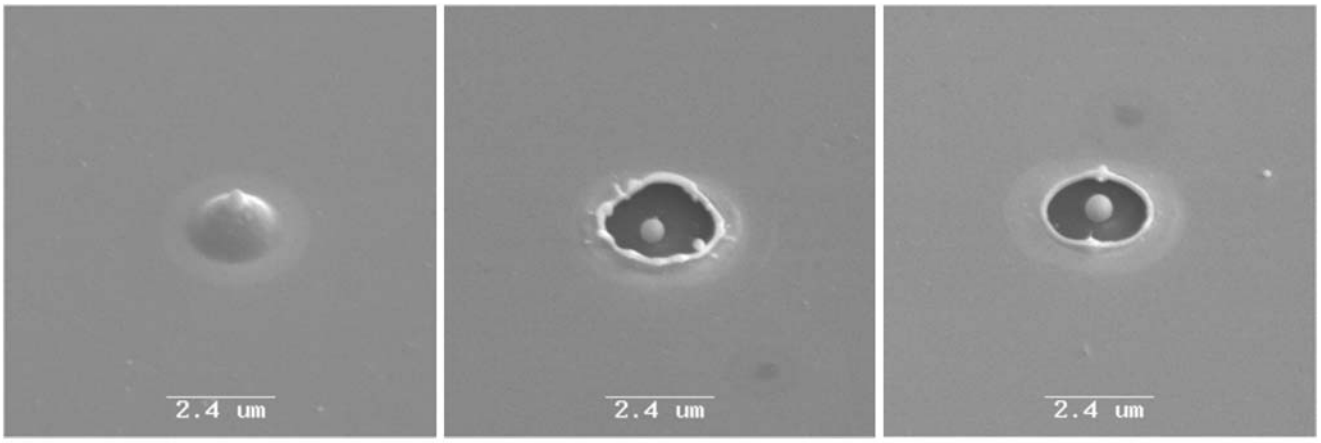

Fig. 6 Structures obtained after irradiation of a 60 nm gold film by a single (**a**) and two delayed by 1 ms (**b**) and 3 s (**c**) femtosecond laser pulses with the pulse energy of 50 nJ. The laser beam with the diameter of 8 mm has been focused on the sample surface with a 20 mm achromatic lens

created structures (see Figs. 4(d) and 3(c)) is determined by the competition between the melted material flow, induced by the thermal expansion, and the surface tension. However, the observed smaller droplet size in the center of the irradiated region and presence of small droplets at the edges (see Fig. 6(b)) can also indicate that after the second pulse a partial reversal of melted flow exists and the impurity-dependent surface tension gradients cannot be completely excluded from the consideration.

Another important feature of the fabricated structures is the appearance of hollow bump at low laser intensities. The bump size first grows with the laser fluence up to a certain level (see profiles in Fig. 2(b)) and then starts to decrease. In the last case, redistribution of the melted material from the edges to the center of the irradiated region occurs. Such behavior is observed for all types of the fabricated structures (see Figs. 2, 3, and 4). One can suggest that the bump is formed due to the plastic deformation of the film induced by the thermal material expansion as it was proposed in [21].

Taking into account the thermo-induced plastic deformation of the solid film and the discussed above melted material dynamics, one can explain the main features of the fabricated structures. Femtosecond laser irradiation results in fast material heating and partial melting. As it was shown in [21], the nanojet formation starts when the intensity is high enough and material melts in the center. Our experimental results show that the metal film is only partially melted and this melt undergoes redistribution (see, for example, Figs. 3(c) and 4(d)). The unmelted part of the film expands due to the laser-induced thermal stress, working like a piston, and pushes the melted material into the center of the irradiated region (see the scheme in Fig. 5(a)). Also changes in the material density induced by the solid–liquid phase transition support this process. The expanding liquid can be reflected from the structural edges running a wave to the center. Therefore, there are at least two reasons why the melted material moves towards the central part of the irradiated region (Fig. 5(b)). The heated part underneath, which remained solid, swells up due to the plastic deformation induced by the thermal stress (Fig. 5(c)). Simultaneous redistribution of the melted material and swelling of the solid film can explain the formation of the observed microbump/nanojet structures shown in Fig. 4(b) and 4(c). At relatively high laser fluences, the unmelted part of the film becomes very thin, and therefore does not have sufficient mechanical strength to create a stable bump.

In order to support the proposed mechanism, changes in the optical reflection of a probe beam by the irradiated area have been measured. For this purpose the beam of a green cw laser (Verdi V10, Coherent) was focused from a side onto the irradiated area. The reflected beam was focused onto a fast photo-diode, which signal was displayed by a 500 MHz digitizing oscilloscope (Tektronix). The oscilloscope was trigged by a femtosecond laser pulse and recorded changes in the reflection of probe beam with nanosecond time resolution. Femtosecond laser pulses with beam diameter of 8 mm were focused onto the sample surface by a 60 mm achromatic lens in order to fabricate sufficiently big structure for reproducible reflection measurements. Results of this experiment, as well as the corresponding structures fabricated on the gold film surface, are shown in Fig. 7. One can see from this figure that the characteristic time scale for the observed changes in reflection is of the order of 50 ns. These changes can be addressed to the appearance of melted material and its movement towards the center. Taking into account that the radius of the melted area is 3 μm, one can estimate the average velocity of the melted material flow as 60 m/s. According to the proposed mechanism, the melted material is accelerated up to this velocity due to the thermal expansion of the unmelted solid material at the structural

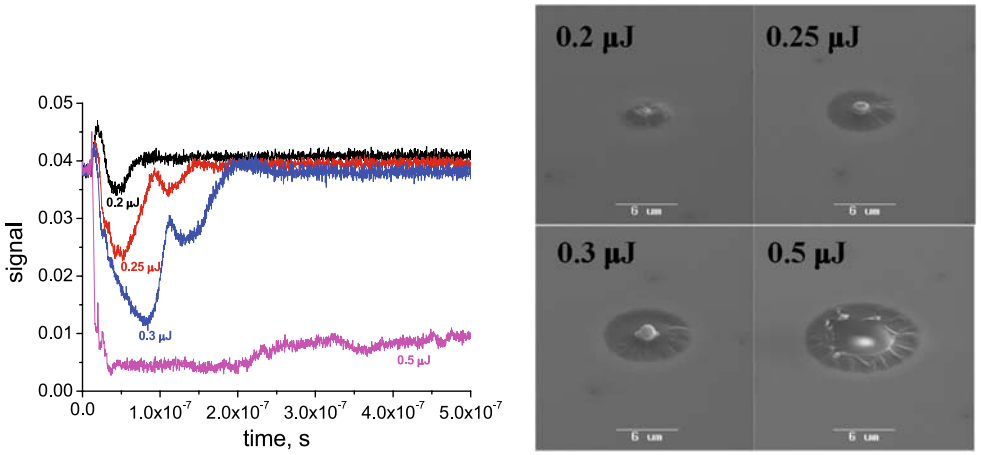

Fig. 7 Optical reflection changes of a 60 nm gold film irradiated by single femtosecond laser pulses (*left*). The laser pulse energies are shown in the figure. SEM images of the fabricated structures (*right*)

edge ("walls" at the solid–liquid interface, see Fig. 5). The characteristic time for the material heating and expansion is determined by the electron–phonon energy transfer and is of the order of 50 ps [21]. In order to provide the required acceleration of the melted material towards the center and the flow velocity of 60 m/s, thermal material expansion of the solid "walls" (also directed to the center) in 50 ps should be of the order of $\Delta L = 60\ \text{m/s} \times 50\ \text{ps}/2 = 1.5$ nm. One can estimate the thickness of the heated layer, which can expand on 1.5 nm, taking into account the coefficient of linear thermal expansion of gold $\alpha = 14.2 \times 10^{-6}\ \text{K}^{-1}$ and the melting temperature $T_m = 1336$ K [21], as follows:

$$L = \Delta L/\alpha \times \Delta T = \Delta L/\alpha \times (T_m - 295\ \text{K}) \approx 100\ \text{nm}.$$

This value coincides with the characteristic electron heat penetration depth [29] and is much smaller than the size of irradiated region. The above estimations show that thermal expansion of the heated "walls" around the melted pool, in case of femtosecond laser irradiation, can initiate strong redistribution of the melted material and result in the formation of the observed structures.

Liquid gold accelerated to the center produces the nanojet which size is determined by the surface tension forces. The energy balance for this process can be roughly expressed as $mV^2/2 = W_{surf}$, where m and V are, correspondingly, the mass and initial velocity of the liquid gold; W_{surf} is the mechanical work against the surface tension forces. Here, all friction forces are neglected and it is assumed that the solidification process starts when the velocity of liquid is close to zero.

Taking the density of liquid gold $\rho = 17.4\ \text{g/cm}^3$ [24] and the initial velocity $V = 60$ m/s, the radius of the melted area $R = 1.5$ μm (for the jet in Fig. 4(d)) and the thickness of the melted layer $l \approx 20$ nm (calculated from the volume of the jet in Fig. 4(d)), one can estimate the initial kinetic energy of the liquid as: $mV^2/2 = \rho \times \pi R^2 \times l \times V^2/2 \approx 4 \times 10^{-12}$ J. In order to roughly estimate the mechanical work of the surface tension forces, $F_{surf} = 2\pi r \times \sigma$, where r is the radius of the small droplet on the top of the nanojet (see Fig. 4(d)) and σ is the surface tension, we multiply it by the height of the nanojet h_{jet}:

$$W_{surf} \approx 2\pi r \times \sigma \times h_{jet} \approx 2 \times 10^{-12}\ \text{J},$$

where $\sigma = 1.1$ N/m is the surface tension of liquid gold [30], whereas $r = 0.25$ μm and $h_{jet} = 1.4$ μm are taken from Fig. 4(d).

The estimated value of the mechanical work of the surface tension forces is of the same order of magnitude as the initial kinetic energy of the liquid gold. This proves that the formation of the observed nanojet structures can be explained by the melted material flow towards the center, which is trigged by the thermal expansion of the solid walls, subsequent jet formation, which is arrested by the surface tension forces, and material solidification.

The reflection curves shown in Fig. 7 demonstrate some oscillations. The presence of these oscillations is not fully understood and can indicate more complex dynamics of the liquid flow. The time period of these oscillations is of the order of 50 ns and is close to the period of thermocapillary waves found after nanosecond laser irradiation [5, 6].

An interesting illustration of the observed phenomena is the material behavior during the irradiation of the gold film by a single femtosecond laser pulse with a ring-shaped intensity distribution (Fig. 8). One can see in this figure that at low laser energies the gold film forms a ring-shaped bump (Fig. 8(a)) and at slightly higher laser energies the ring-shaped area of melted material (Fig. 8(b)). At the inner and outer edges of the melted ring there appear forces due to the thermal expansion of the surrounding heated metal "walls". It is clear that the force acting on the outer edge (due to the longer interface length) will be higher than that acting on the inner edge. Therefore, the melted material will be redistributed from the outer ring edge towards the inner ring edge as can be seen in Fig. 8(b) and Fig. 10(a). This difference

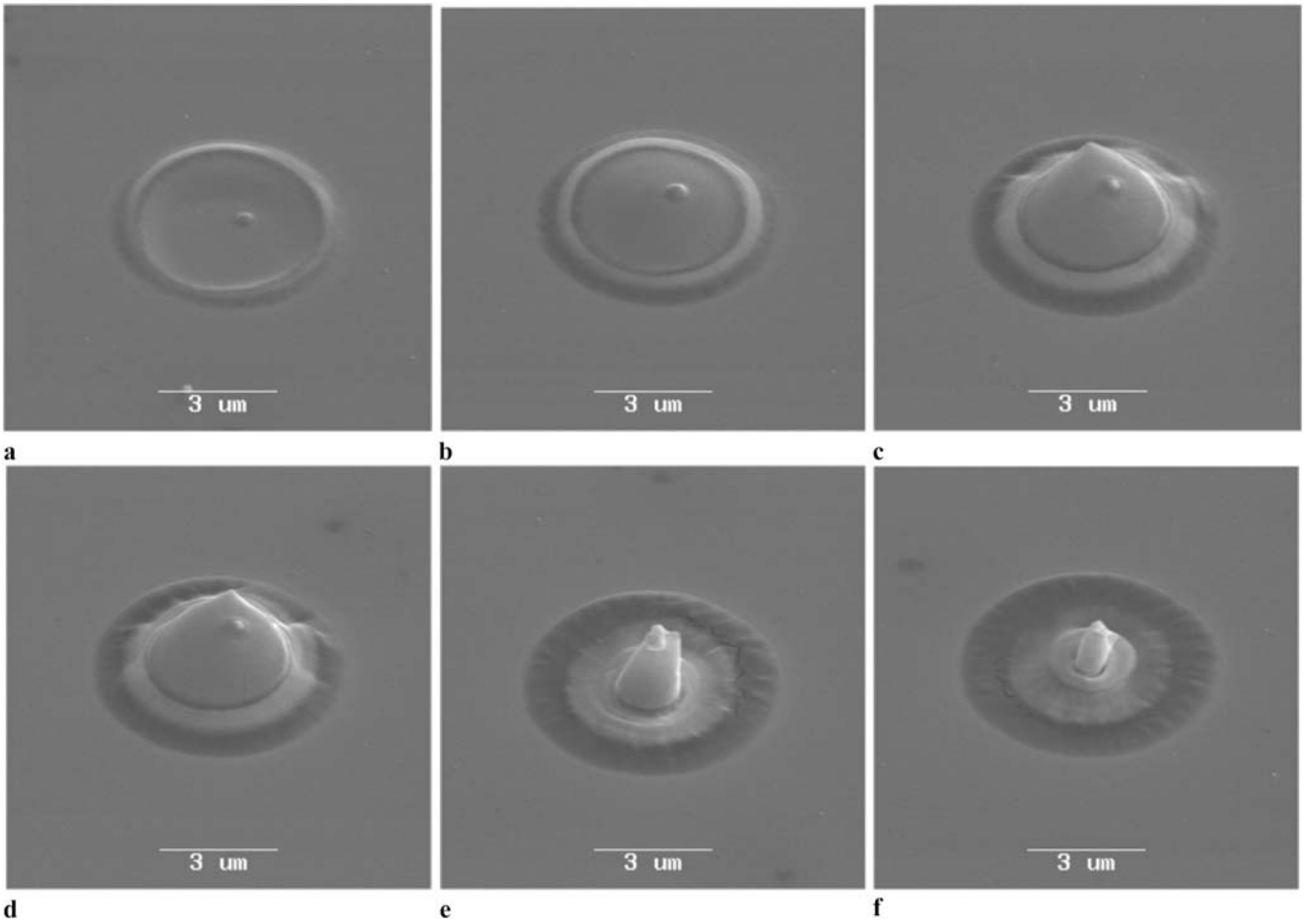

Fig. 8 Structures obtained after irradiation of a 60 nm gold film by single femtosecond laser pulses with a ring-shaped intensity distribution. The laser pulse energies were 75 μJ (**a**), 85 μJ (**b**), 90 μJ (**c**), 95 μJ (**d**), 105 μJ (**e**), and 110 μJ (**f**). The field distribution on the sample surface has been created by an image transfer (at 50× demagnification) of a ring-shaped mask with the 260 μm external and 160 μm internal diameters

in the forces acting on the ring edges grows with the laser energy and leads to the overall flow of the melted material towards the ring center (Fig. 8(c) and 8(d)). At these laser fluences, the film in the ring center is swelled. This swelling appears due to the melted ring induced forces and due to the heating of solid material in the central part. At higher laser fluences the melted material proceeds further to the ring center and squeezers the unmelted gold film in the central part (Fig. 8(e) and 8(f)). In Fig. 8(f), one can see the ring formed by the melted material and the compressed unmelted gold film in the center.

3.2 Resolution limits

In the previous part, it has been shown that microstructures with a controllable nanorelief can be fabricated by femtosecond laser irradiation of gold films using different laser intensity distributions. In order to study the resolution limits of this technique, an image transfer of the variable slit diaphragms has been performed with a 50× demagnification. This procedure results in a flat-top, line-like intensity profile on the sample surface. At relatively high laser fluences ($F \geq 0.2$ J/cm^2) this intensity profile induces melting of the gold film and redistribution of the melted material from the edges to the center of the irradiated line region (see Fig. 9(b)–(e)). Dependence of the thickness of the fabricated lines d_{line} on the width of the laser intensity distribution on the sample surface d_{field} is shown in Fig. 9(a) by the filled squares. d_{field} has been calculated as the thickness of the diaphragm divided by the corresponding demagnification factor. One can see that at a relatively broad intensity distribution, $d_{field} \geq 3$ μm, the thickness of the fabricated lines d_{line} is proportional to d_{field} and is about 6.5 times smaller. For $d_{field} < 3$ μm, the thickness of the fabricated line is almost constant of the order of 300–400 nm. In order to verify that this limitation is not due to the diffraction limit of the optical system the image transfer experiments with a 100× demagnification have been performed.

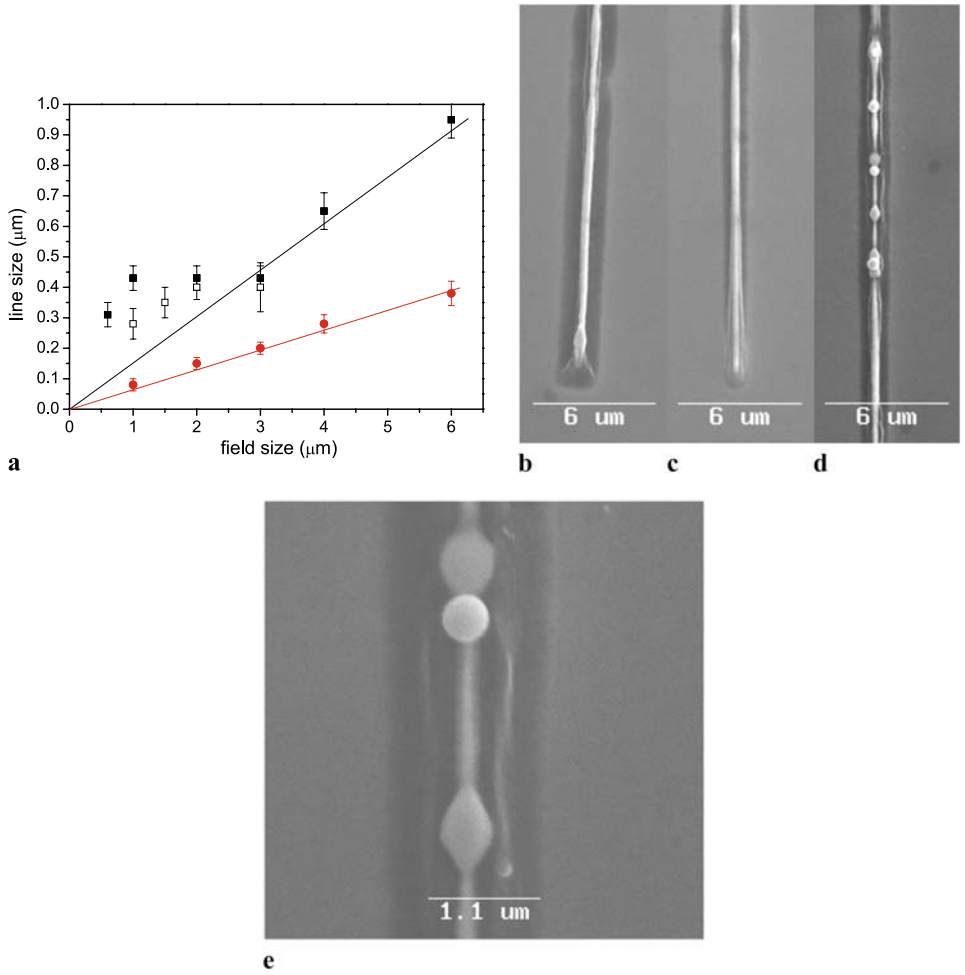

Fig. 9 (**a**) Dependence of the thickness of fabricated lines on the width of laser intensity distribution on the sample surface. *Filled squares–regular lines*, *filled circles–thin lines* obtained at higher laser intensities close to the ablation threshold. The slit image is transferred with a 50× demagnification. *Empty squares–regular lines* fabricated by an image transfer with a 100× demagnification. (**b**)–(**e**) Examples of lines fabricated by an image transfer with the 50× demagnification of 150 μm (**b**) and 100 μm (**c**)–(**e**) slits. Image (**d**) shows a thin line with the droplets on the top. Image (**e**) is the magnified fragment of Image (**d**)

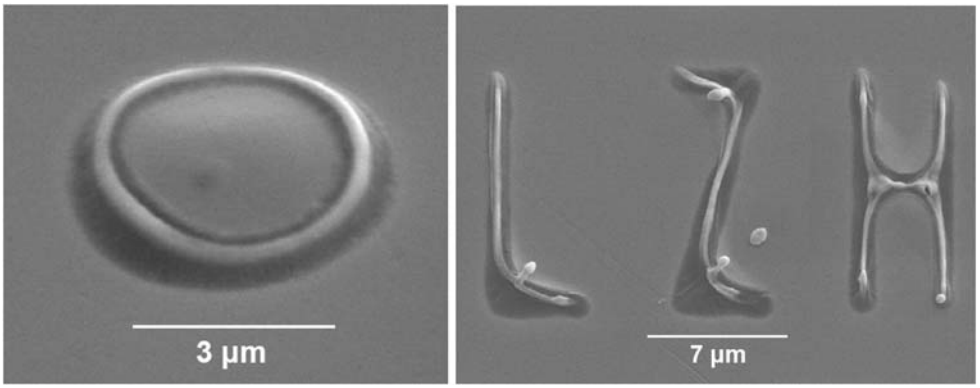

Fig. 10 Examples of structures fabricated on a 60 nm gold film surface by single femtosecond laser pulses. Images of the corresponding masks have been transferred onto the sample surface with the 50× demagnification

Results of these experiments are shown in Fig. 9(a) by empty squares. One can see that the minimum thickness of controllably formed lines obtained in this case is almost the same as in the previous experiments with the 50× demagnification. As it was mentioned above, these lines are hollow inside and look like a bump structure. At laser fluences close to the ablation threshold $F_{th} \approx 0.25\ \mathrm{J/cm^2}$, the bump structure can be broken. This process leads to the formation of thinner lines with multiple droplets on the top (see Fig. 9(d), (e)). Dependence of the thickness of these thinner lines d_{line} on d_{field} is shown in Fig. 9(a) by filled circles. One can see that d_{line} is proportional to d_{field} and is about 15 times smaller. The minimum thickness of this line observed in our experiments is about 80 nm.

Examples of more complex structures, which can be fabricated by a single femtosecond laser pulse irradiation, are

shown in Fig. 10, demonstrating that also interconnected structures can be produced.

4 Conclusion

Nano- and microstructuring of thin gold films by femtosecond laser pulses have been studied. It has been shown that different types of microstructures can be fabricated by single femtosecond laser pulses with a controlled laser intensity profile. Desired micro-intensity distributions on the sample surface have been produced by an image transfer of special masks with a 50× demagnification. These masks have been fabricated by femtosecond laser ablation of a chromium film deposited onto a glass substrate.

The demonstrated microstructures in gold films are formed due to the laser-induced dynamics of the melted material and film swelling. Redistribution of the melted material in the irradiated region from the edges to the center has been observed. These and other effects responsible for the formation of microstructures have been discussed.

Using this technique, 300–400 nm homogeneous lines can be controllably fabricated on the gold film surface. Moreover, close to the ablation threshold as thin as 80 nm lines can be formed, which are not homogeneous and have nanodroplets on their top.

Acknowledgements The authors thank Alexander von Humboldt Foundation for financial support of Arseniy Kuznetsov.

References

1. F. Korte, J. Serbin, J. Koch, A. Egbert, C. Fallnich, A. Ostendorf, B.N. Chichkov, Appl. Phys. A **77**, 229 (2003)
2. J. Koch, E. Fadeeva, M. Engelbrecht, C. Ruffert, H.H. Gatzen, A. Ostendorf, B.N. Chichkov, Appl. Phys. A **82**, 23 (2006)
3. A.P. Joglekar, H. Liu, G.J. Spooner, E. Meyhöfer, G. Mourou, A.J. Hunt, Appl. Phys. B **77**, 25 (2003)
4. Yu. Kaganovskii, H. Vladomirsky, M. Rosenbluh, J. Appl. Phys. **100**, 044317 (2006)
5. V.Yu. Balandin, U. Gernert, T. Nink, O. Bostanjoglo, J. Appl. Phys. **81**, 2835 (1997)
6. O. Bostanjoglo, T. Nink, Appl. Surf. Sci. **109/110**, 101 (1997)
7. F. Korte, J. Koch, B.N. Chichkov, Appl. Phys. A **79**, 879 (2004)
8. J. Koch, F. Korte, T. Bauer, C. Fallnich, A. Ostendorf, B.N. Chichkov, Appl. Phys. A **81**, 325 (2005)
9. Y. Nakata, T. Okada, M. Maeda, Jpn. J. Appl. Phys. **42**, L1452 (2003)
10. Y. Nakata, N. Miyanaga, T. Okada, Appl. Surf. Sci. **253**, 6555 (2007)
11. V.S. Ajaev, D.A. Willis, Phys. Fluids **15**, 3144 (2003)
12. C. Favazza, J. Trice, R. Kalyanaraman, R. Sureshkumar, Appl. Phys. Lett. **91**, 043105 (2007)
13. J. Trice, D. Thomas, C. Favazza, R. Sureshkumar, R. Kalyanaraman, Phys. Rev. B **75**, 235439 (2007)
14. C. Favazza, R. Kalyanaraman, R. Sureshkumar, Nanotechnology **17**, 4229 (2006)
15. E. Haro-Poniatowski, E. Fort, J.P. Lacharme, C. Ricolleau, Appl. Phys. Lett. **87**, 143103 (2005)
16. J.E. Kline, J.P. Leonard, Appl. Phys. Lett. **86**, 201902 (2005)
17. A. Lasagni, C. Holzapfel, F. Mücklich, Appl. Surf. Sci. **253**, 1555 (2006)
18. A. Rosenfeld, E.E.B. Campbell, Appl. Surf. Sci. **96–98**, 439 (1996)
19. Y. Nakata, T. Okada, M. Maeda, Opt. Lasers Eng. **42**, 389 (2004)
20. S. Preuss, A. Demchuk, M. Stuke, Appl. Phys. A **61**, 33 (1995)
21. Y.P. Mescheryakov, N.M. Bulgakova, Appl. Phys. A **82**, 363 (2006)
22. D.S. Ivanov, L.V. Zhigilei, Phys. Rev. B **68**, 064114 (2003)
23. N. Seifert, G. Betz, W. Husinsky, Appl. Surf. Sci. **96–98**, 33 (1996)
24. N. Seifert, G. Betz, W. Husinsky, Appl. Surf. Sci. **103**, 63 (1996)
25. R. Kelly, J.E. Rothenberg, Nucl. Instrum. Methods Phys. Res. B **7/8**, 755 (1985)
26. T.D. Bennett, C.P. Grigoropoulos, J. Appl. Phys. **77**, 849 (1995)
27. D.A. Wills, X. Xu, J. Heat Transfer **122**, 763 (2000)
28. M. Iwamoto, M. Ye, C. Grigoropoulos, R. Greif, Num. Heat Transfer A **34**, 791 (1998)
29. S. Nolte, C. Momma, H. Jacobs, A. Tünnermann, B.N. Chichkov, B. Wellegehausen, Welling, J. Opt. Soc. Am. B **14**, 2716 (1997)
30. I. Egry, G. Lohoefer, G. Jacobs, Phys. Rev. Lett. **75**, 4043 (1995)